Available online at www.sciencedirect.com

ScienceDirect

Procedia Structural Integrity 28 (2020) 74–83

Structural Integrity Procedia

www.elsevier.com/locate/procedia

1st Virtual European Conference on Fracture

Stress intensity factors K_I, K_{II}, K_{III}, K_{eq}, induced at the crack tip of CT specimens subjected to torsional loading

Rui F. Martins[a]*, Luís Ferreira[a]

[a]*UNIDEMI, Department of Mechanical and Industrial Engineering, NOVA School of Science and Technology, 2829-516 Caparica, Portugal*

Abstract

The paper herein presented shows the Stress Intensity Factors (SIF), K_I, K_{II}, K_{III}, and K_{eq}, calculated for Compact Tension (CT) specimens with different thicknesses (B), namely 2.5 mm; 3 mm; 5 mm; 7.5 mm, and 10 mm, that were subjected to three torsional loads (T): 6 $N.m$; 7.5 $N.m$; 9 $N.m$. Fatigue pre-crack subjected to torsional loading was found to be predominantly under Mode-II loading, and a crack branch was observed.
The CT specimens, which were analysed using the Finite Element Method (FEM), were then modelled with two cracks that had grown experimentally from a fatigue pre-crack along two directions (+70º and -70º), and for several crack lengths (a/L=0; a/L=0.25; a/L=0.50; a/L=0.75; a/L=1.0). Therefore, equivalent SIF, K_{eq}, were calculated from the numerical results of K_I, K_{II} and K_{III}, and a polynomial regression function was determined in function of the thickness of the specimen (B), the crack length (a/L) and the applied torque (T). It was observed that even in the case of a Mode-III loading is applied, Mode I was locally dominant at the branched crack tip, followed by Mode III and Mode II, in that order of relevance. It was also observed that the maximum equivalent SIF occurred at the two outer lateral surfaces of the CT specimens under test, resulting in high crack growth rates in those locations, and minimum at the midplane of the specimen.

Keywords: Torsional loading; Stress intensity factors; CT specimens; Finite Element Analyses.

* Corresponding author. Tel.: +351-212-948-567; fax: +351-212-948-531.
E-mail address: rfspm@fct.unl.pt

10.1016/j.prostr.2020.10.010

1. Introduction

Fatigue crack growth in mechanical components frequently leads to failure, which, as stated by Collacott (1977), can be of a catastrophic type and result in an immediate inability of a system to achieve its function (Gomes *et al.*, 2018) (Barata *et al.*, 2017) (Infante *et al*., 2003*)* (Branco *et al.* 2002), or in a reducing performance of the equipment (Soares *et al.*, 2019) (Bugio *et al.,* 2013).

Nomenclature

a	Crack length
B	Thickness of the CT specimen
CT	Compact Tension specimen
J-Integral	Line integral around the crack tip (path-independent)
K_I, K_{II}, K_{III}	Stress intensity factor under Mode-I, II, III loading, respectively
K_{eq}	Equivalent stress intensity factor
Pmax	Maximum tensile load applied during fatigue pre-crack
R	Load ratio
W	Width of the specimen
ΔK_I	Stress intensity factor range under Mode-I loading
ΔK_{Ith}	Threshold stress intensity factor range under Mode-I loading
ΔP	Load range
ν	Poisson's coefficient

Those failures are fortunately detected, most of the times, before causing injury or even human death and frequently stress concentrations are the cause of fatigue crack initiation, growth and failure in many industrial components (Beretta *et al.*, 2016), which are also subjected to very complex loading conditions during service (Weiss and Pineau, 1993). Hence, local elastic-plastic stresses and strains around the stress risers are frequently in a multiaxial situation, even under uniaxial loading, being essential to determine the crack path and its growth in critical regions (Ohkawa, 2011).

Cyclic torsion is a common loading mode. In practice, fatigue cracks often show shear mode crack propagation under reversed torsional loading in rotating power trains or force transmission systems in mechanical structures, such as power plants (Tanaka *et al.,* 1996), but also in commonly used engineering components, such as axles and crankshafts that are stressed not only with axial tension-compression loads but also with cyclic torsional loads (Schönbauer *et al.*, 2017). Therefore, the torsional fatigue strength is essential for the design of such mechanical components and has been studied by many researchers who investigated shear mode crack growth in smooth cylindrical specimens (Ohkawa, 2011) (Murakami *et al.*, 2008) (Shimamura *et al.,* 2014) (Murakami *et al.*, 2005), or in circumferential V-notched cylindrical specimens (Pokluda *et al.*, 2010), or in fatigue pre-crack prismatic specimens (Gasiak and Robak, 2010) (Martins *et al.*, 2016), to mention few.

In such cases, after the initial fatigue crack growth under Mode II+III, for which crack initiations occur on planes experiencing the maximum shear stress amplitude (Susmel and Taylor, 2006), crack usually branches by the Mode I crack growth and continues propagation until the specimen fails (Murakami *et al.*, 2008). Moreover, branched angles are close to the direction perpendicular to the local maximum normal tensile stresses (±70.5º) (Murakami *et al.*, 2008), and branching appears at the moment when the maximal ΔKI-value exceeds that of the threshold ΔKI_{th} (Pokluda *et al.*, 2010), since the threshold level for propagation of a Mode-I crack is much smaller than that of a shear-mode crack (Okazaki *et al.*, 2017). In addition, it has been reported that fatigue crack growth rates under shear-mode (modes II and III) may decrease with a crack extension due to sliding interference between crack faces, which can result in crack-tip shielding, friction and mechanical locking of asperities (Okazaki *et al.*, 2017) (Tanaka *et al.,* 1996); in this case, it is necessary to apply higher stress levels to extend the shear-mode crack length and to maintain the effective shear-mode driving force (Gates and Fatemi, 2016).

Additionally, crack growth rates and crack growth path will depend on the type and magnitude of the applied loads, as well as on the thickness of the specimens, the crack length, and the material type, to mention a few. Hence, in general, cracks in the low cycle fatigue regime tend to grow on maximum shear planes while cracks at longer lives tend to branch into Mode-I growth for specimens subjected to pure torsion (Okazaki *et al.*, 2017).

2. Materials and methods

Standard CT specimens are widely used to determine the fatigue crack growth rates (FCGR) of materials subjected to Mode-I loading as a function of crack-tip stress intensity factor range, ΔK_I (ASTM E647). This type of experimental test covers the FCGR from the near-threshold stress intensity factor range of the material, ΔK_{Ith}, to the maximum stress intensity factor (K_{max}), which is an approximate value for its fracture toughness. Therefore, the stress intensity factor formulation at the crack tip is a very well-known mathematical formulation that is expressed in function of the load range (ΔP), the geometry of the CT specimen (B, W) and the crack length (a) (Fig. 1a).

During the research herein presented, thin sheet standard CT specimens (Fig. 1b), made of an AISI 316L austenitic stainless steel (Table 1) (Martins and Branco, 2004), and with a thickness (B) equal to 3 mm, were tested, under torsional load, using a bi-axial servo-hydraulic *Instron 8874* machine (Fig. 1c). Previously, Mode-I fatigue pre-cracks were propagated in the CT specimens approximately 2 mm away from the V-notch root (Fig. 1d), so that the crack tip could overcome the plasticized region generated during the machining process of the notch (P_{max}=2500 N, R=0.1, under constant amplitude loading, during approximately 50 000 cycles).

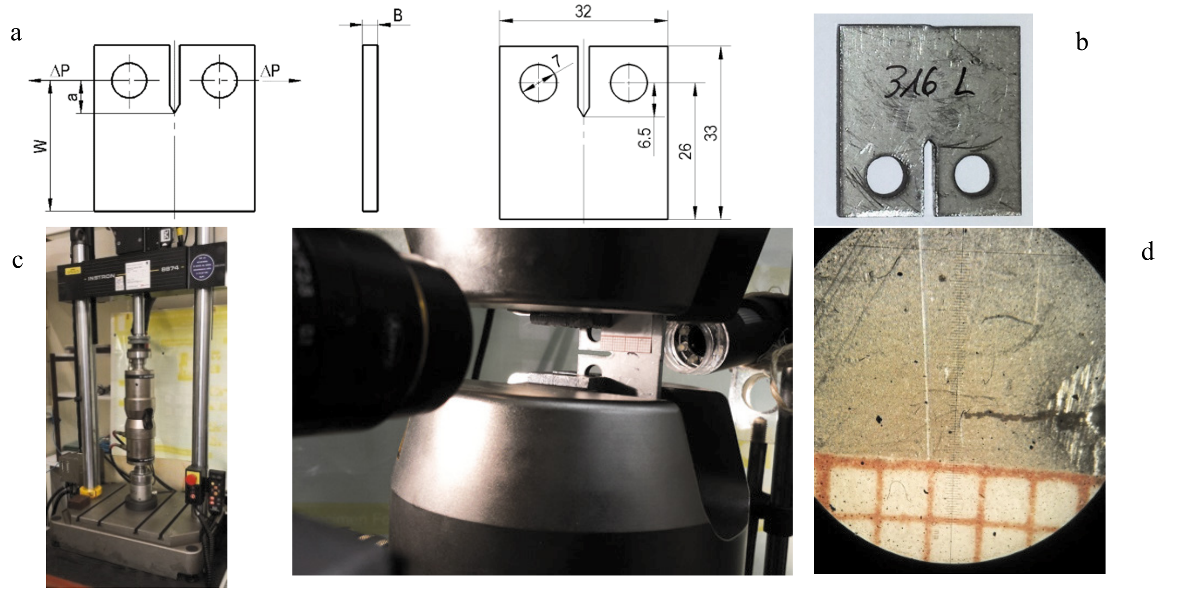

Fig. 1. (a) Main dimensions of a CT specimen; (b) Dimensions, in millimetres, of the CT specimen under test; (c) Bi-axial servo-hydraulic Instron 8874 machine; (d) Magnified view of the fatigue pre-crack propagated under Mode-I loading from the V-notch root of CT specimens.

Table 1. Chemical composition and mechanical properties of AISI 316L at room temperature (Martins and Branco, 2004).

	C (%)	Mn (%)	Cr (%)	Ni (%)	Mo (%)	N (%)	Si (%)	Cu (%)	V (%)	P (%)	S (%)
AISI 316L	<0.05	1.30	17.34	11.11	2.23	0.08	0.37	0.22	0.07	0.03	0.004

	Tensile Strength (MPa)	Yield Strength (MPa)	Ductility, ε [mm/mm]
AISI 316L	600	290	Higher than 50% at room temperature

A typical fracture surface obtained after the application of torsional loading is presented in figure 2, and extra experimental details can be found in (Martins *et al.*, 2016). From the observation of figure 2, crack branch occurred after the application of a reduced number of cycles along with two deflection angles of about ±70º; in addition, crack growth occurred preferentially at the outer surfaces towards the midplane.

Concerning the calculation of the stress intensity factors present at crack tip of the CT specimens under test, namely K_I, K_{II} and K_{III}, those were calculated through Finite Element Analyses (FEA), using ANSYS Workbench simulation software, for CT specimens with different thicknesses, namely 2.5 mm; 3 mm; 5 mm; 7.5 mm, and 10 mm, that were subjected to three torsional loads: 6 N.m; 7.5 N.m; 9 N.m.

The CT specimens were modelled with two cracks that had grown from a fatigue pre-crack along with two directions (+70º and -70º), and for several crack lengths (a/L=0; a/L=0.25; a/L=0.50; a/L=0.75; a/L=1.0) (Fig.3). The material model was defined as elastic, homogenous and isotropic, with a Young's Modulus equal to 200 GPa and a Poisson's ratio equal to 0.3. Therefore, equivalent stress intensity factor values were calculated from numerical results of K_I, K_{II} e K_{III}, and a polynomial regression function was fitted in function of the thickness of the specimen, the crack length and the applied torque. Stress intensity factors were calculated at each crack tip, at nodes placed across the specimen's thickness, and at six contours/per node, only considering J-integral values that shown to be independent of contour.

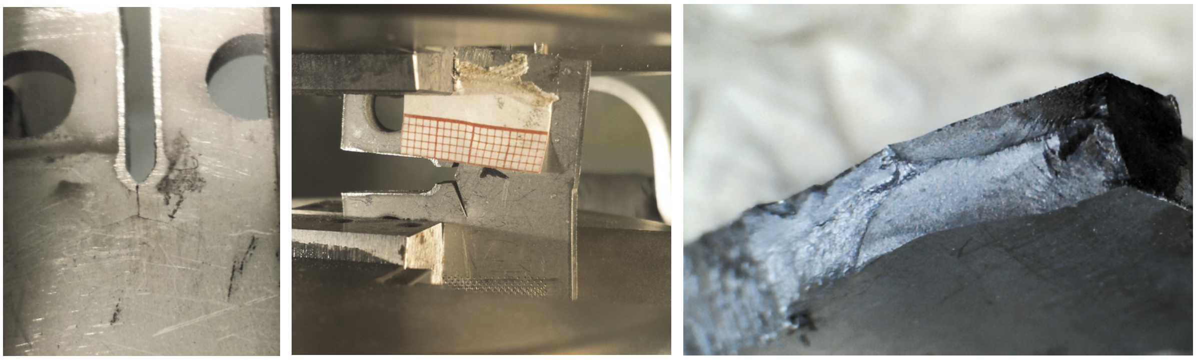

Fig. 2. CT specimen under torsional loading (R=-1): crack branch and overall view of a typical fracture surface obtained.

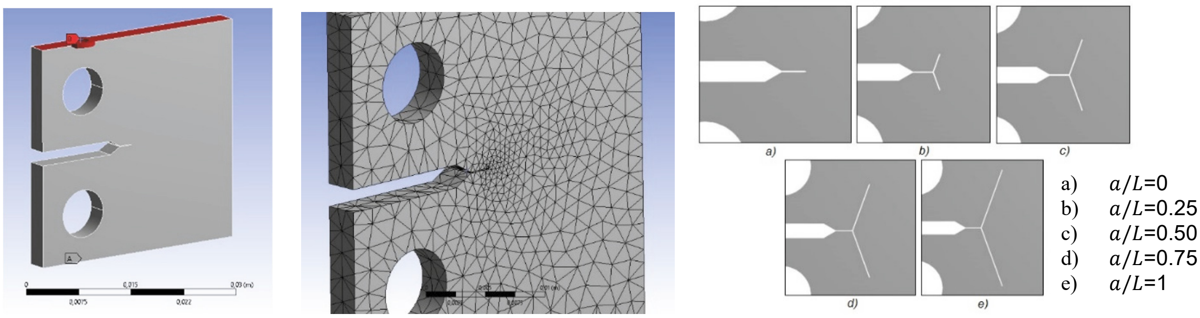

Fig. 3. Pre-cracked CT specimen (a/L=0) with its finite element mesh defined. Crack growth simulation along +70º and -70º, for several crack lengths, namely a/L=0; a/L=0.25; a/L=0.50; a/L=0.75; a/L=1.0.

3. Results and its discussion

3.1. Pre-cracked specimens under torsional loading (a/L=0): are they really under Mode-III loading?

When a fatigue pre-crack CT specimen (Fig. 3) is subjected to torsional loading, the crack tip is expected to be mainly submitted to shear stresses and crack growth to occur under shear mode loading. For this type of load case, a through-thickness semi-elliptical crack was inserted in the numerical model under analysis (Fig. 4a), coplanar with the fatigue pre-crack, and a 5 N.m torque was applied to the upper surface of the specimen (Fig. 3). The stress intensity factors acting at the crack tip were calculated and are presented in Fig. 4b, c and d.

From the analysis of the numerical results obtained, it can be concluded that:

- At the midplane of the CT specimen, K_I and K_{II} values are equal to 0 MPa.m$^{0.5}$ (Fig. 4b, c), and K_{III} shows a maximum value of approximately 3.6 MPa.m$^{0.5}$ (Fig. 4d). Moreover, K_{III} values along the crack tip oscillate between maximum and minimum values making suppose that there are some points at the crack tip more prone to propagate than others under Mode-III loading (Fig. 4d);

- K_I and K_{II} values vary almost linearly across the thickness of the CT specimen, showing maximum values at the outer surfaces of the specimen, namely 1.25 MPa.m$^{0.5}$ and 8.6 MPa.m$^{0.5}$, respectively (Fig. 4b, c);
- The SIF values calculated are, despite two points located near the two outer surfaces, independent from the contour and show approximately the same values across the thickness of the specimen (Fig. 4b, c, and d);
- K_{II} is the maximum SIF applied to the CT specimen (8.5 MPa.m$^{0.5}$) (Fig. 4c); hence, crack initiation should be Mode-II dominated and crack should grow a short distance on planes of maximum shear. Nevertheless, the maximum tangential stress criterion would predict the crack initiated under pure torsion loading to immediately branch at an angle of 70.5º to the crack growth direction and grow in Mode I regardless of the applied loading magnitude (Gates and Fatemi, 2016). This type of growth was verified experimentally, as supported by Fig. 2.

a

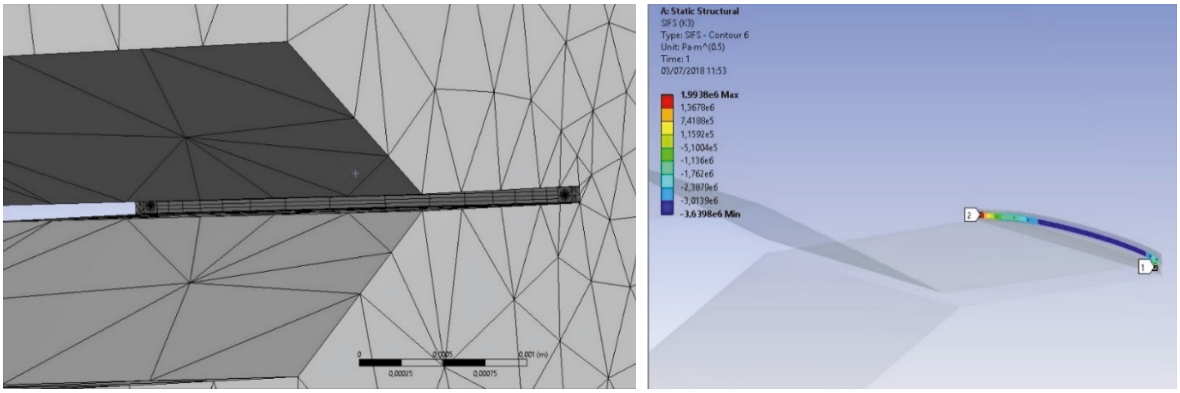

b

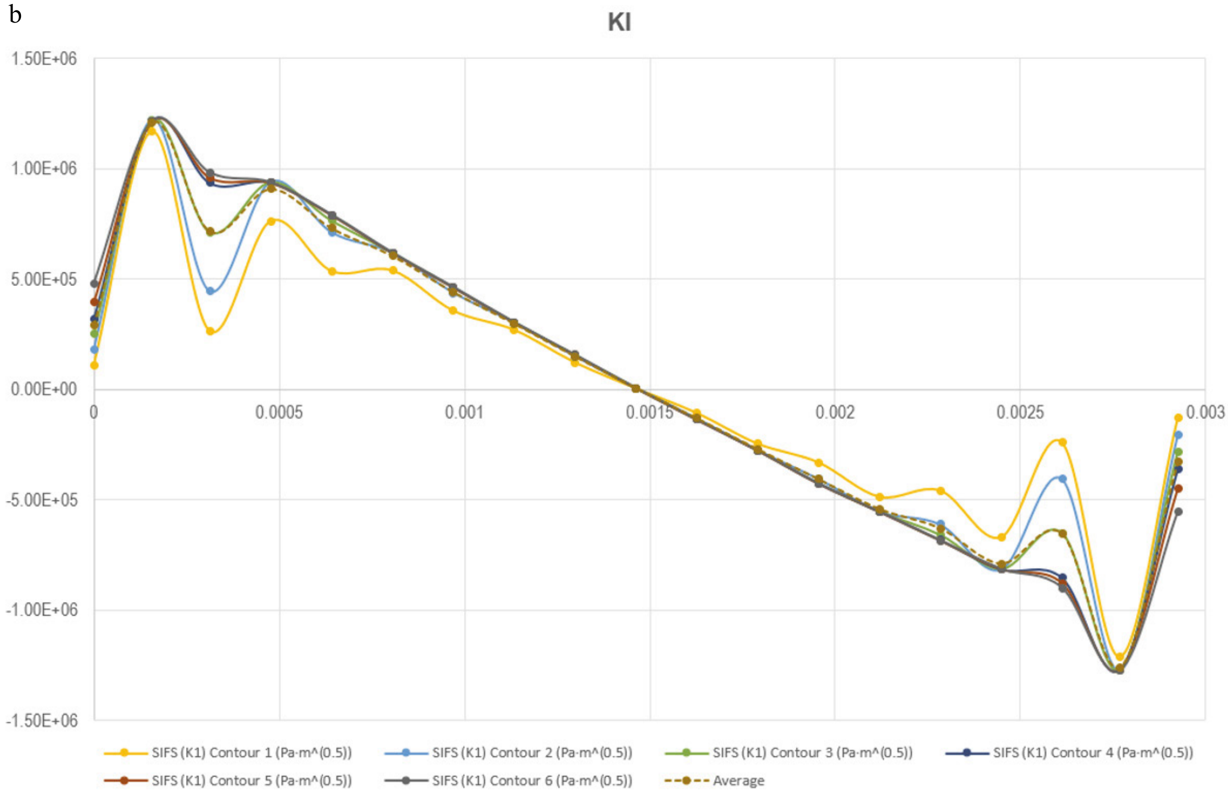

c

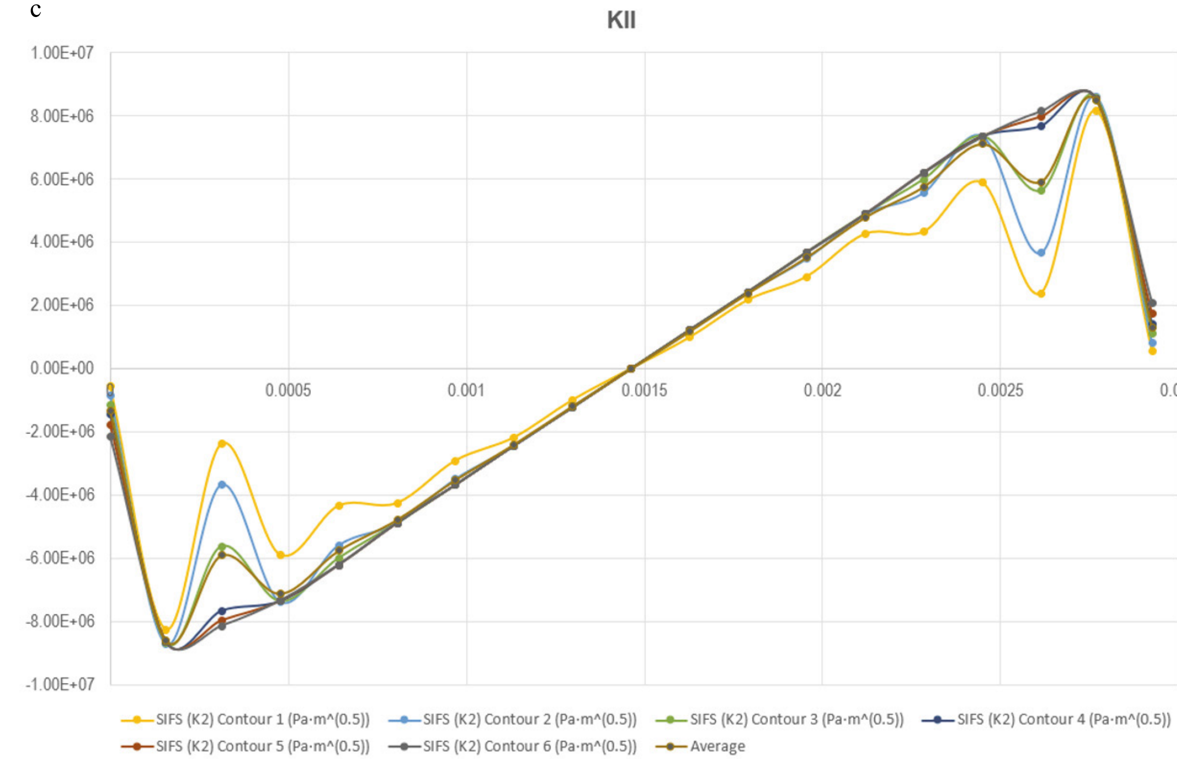

d

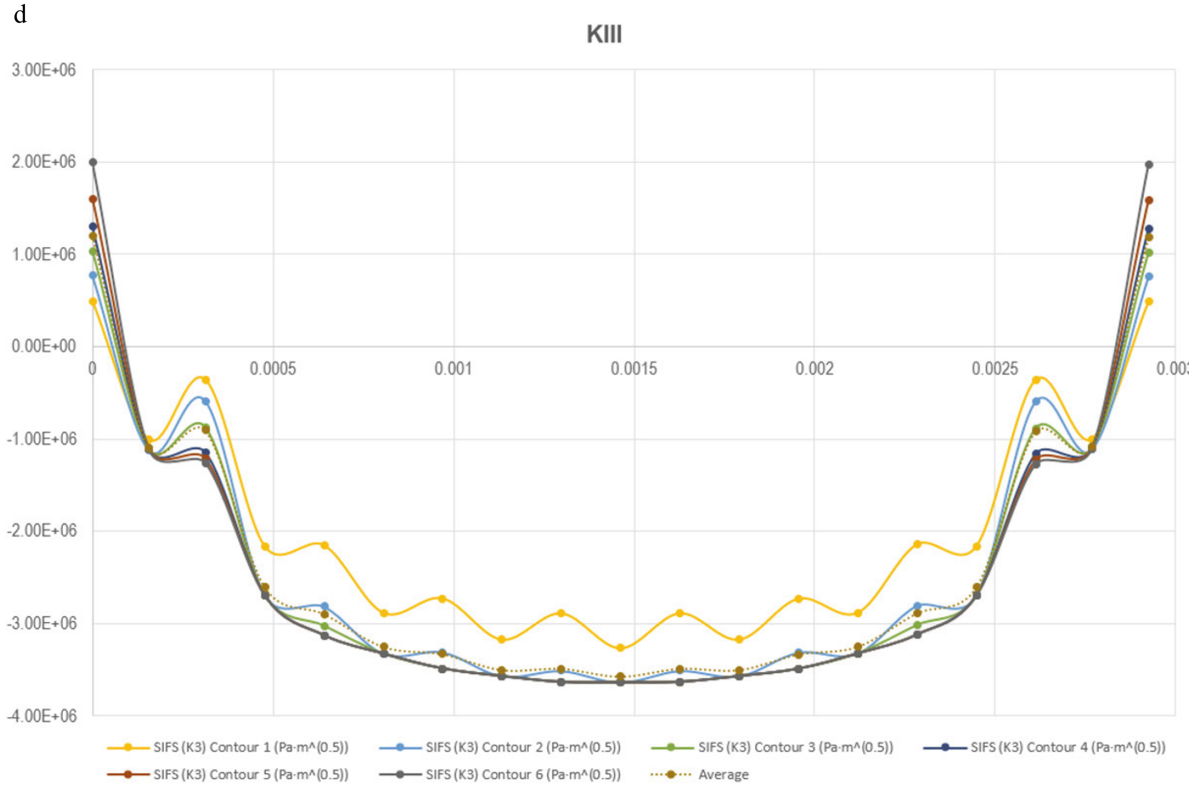

Fig. 4. (a) Overall view of the through-thickness fatigue pre-crack with semi-elliptical shape inserted in the numerical model (a/L=0); (b) Mode-I stress intensity factor (SIF) values, K_I [Pa.m$^{0.5}$], calculated along the thickness of the specimen (x-axis) at six contours; (c) Mode-II stress intensity factor (SIF) values, K_{II} [Pa.m$^{0.5}$], calculated along the thickness of the specimen (x-axis) at six contours; (d) Mode-III stress intensity factor (SIF) values, K_{III} [Pa.m$^{0.5}$], calculated along the thickness of the specimen (x-axis) at six contours.

In addition, considering the Pook's Criterion (Richard *et al.*, 2004) (ν=0.3, Eqs. (1) and (2)), the results presented in Figure 4 allowed to calculate an equivalent stress intensity factor, K_{eq} (Fig.5). From the observation of the results, it can be concluded that a minimum value of K_{eq} will be induced at the midplane of the CT specimens (R=-1) and crack propagation will tend to occur mainly at the outer surfaces of the specimens where K values are maximum.

$$K_{eqI,II} = \frac{0.83K_I + \sqrt{0.4489K_I^2 + 3K_{II}^2}}{1.5} \quad (1)$$

$$K_{eqI,II,III} = \frac{K_{eqI,II}(1+2\nu) + \sqrt{K_{eqI,II}^2(1-2\nu)^2 + 4K_{III}^2}}{2} \quad (2)$$

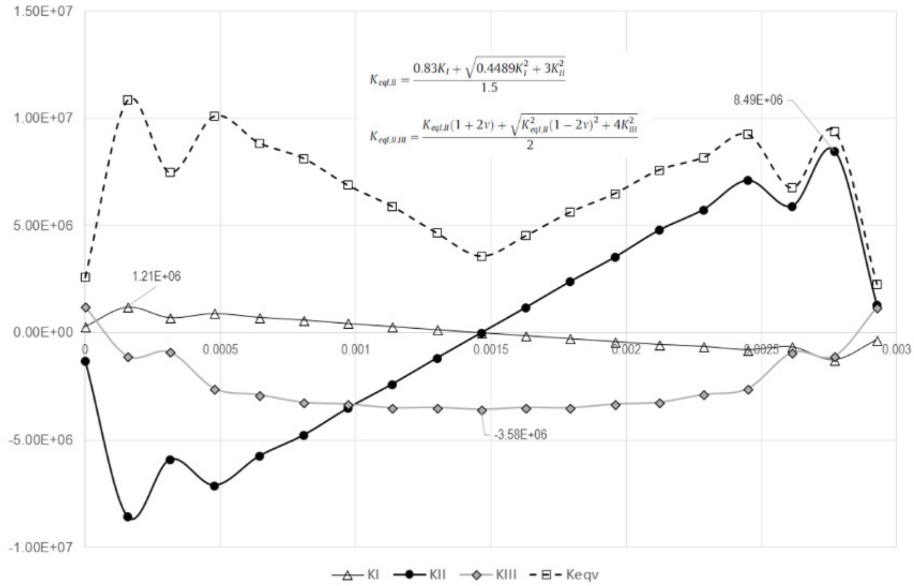

Fig. 5. Stress intensity factors (SIF), K_I, K_{II}, K_{III} and K_{eq}, at the crack tip of a fatigue pre-crack (a/L=0) located in a CT specimen under torsional loading. X-axis represents the thickness of the specimen, B and Y-axis are in $Pa.m^{0.5}$.

3.2. CT specimens under torsional loading

Seventy-five numerical analyses were carried out to determine the SIF acting at the crack tip of CT specimens with five different thicknesses (2.5, 3, 5, 7.5 and 10 mm), under three torque values applied (6.0, 7.5 and 9.0 N.m), and considering five crack lengths (a/L=0, a/L=0.25, a/L=0.5, a/L=0.75, a/L=1). The results obtained throughout the analyses shown a similar trend and only varied in what the values concerned. Therefore, in figure 6, four graphics representing K_I, K_{II}, K_{III} and K_{eq} (Pook) are presented considering a specimen with a thickness equal to 2.5 mm under a torque value of 6 N.m. Once crack branch occurs (Fig. 6), K_I becomes the highest values applied at crack tip (17 $MPa.m^{0.5}$); hence, cracks will tend to grow in Mode-I, on maximum tensile planes, with higher FCGR at the external surfaces of the CT specimen. Moreover, it can be seen from K_I, K_{eq} (Pook) and K_{III} values calculated, that crack growth will tend to decelerate from a/L=0 to a/L=0.25 and then to accelerate from crack length a/L=0.25 to a/L =1.0. Additionally, K_{III} values were almost constant across the thickness of the specimen, presenting maximum value when a/L=0 (5 $MPa.m^{0.5}$) and showed lower values during fatigue crack propagation. Moreover, K_{II} values tended to increase with crack growth and always showed the highest values at the external surfaces of the specimen; nevertheless, their values always remained lower than 3 $MPa.m^{0.5}$ (for a/L=1.0); this contrasts with the higher K_{II} values calculated during shear crack growth (Mode II) when propagated crack remained coplanar with fatigue pre-crack and K_{II} value was about 8.5 $MPa.m^{0.5}$ (Figs. 4a, c). Finally, K_I and K_{II} values varied linearly across the thickness of the specimen, being equal to 0 $MPa.m^{0.5}$ at the midplane (Fig. 6).

For the different thicknesses and torques applied during this investigation, the results of the SIF obtained in the numerical analyses have shown a similar trend as described earlier in Fig. 6 and only varied in what the values concerned. Specifically, it was noticed higher stress intensity factor values with increasing torque applied and a decrease of the stress intensity factors with the increase of the thickness of the specimens. Hence, considering the maximum equivalent stress intensity values, K_{eq} MPa.m$^{0.5}$, calculated for each specimen's thickness (B, in mm), crack length (a/L), and applied torque (T, in N.m), several polynomial functions (Eq. 3) (Table 2) and surface response functions were determined. Moreover, to determine the p_{ij} coefficients of Eq. 3, for the considered torques, a quadratic polynomial equation was fitted, and p_i coefficients were calculated (Eq. 4) (Table 2).

$$Keq(a/L,B) = p_{00} + p_{10}.(\frac{a}{L}) + p_{01}.B + p_{20}.\left(\frac{a}{L}\right)^2 + p_{11}.(\frac{a}{L}).B + p_{02}.B^2 + p_{30}.\left(\frac{a}{L}\right)^3 + p_{21}.\left(\frac{a}{L}\right)^2.B + p_{12}.(\frac{a}{L}).B^2 + p_{03}.B^2 + p_{40}.\left(\frac{a}{L}\right)^4 + p_{31}.\left(\frac{a}{L}\right)^3.B + p_{22}.\left(\frac{a}{L}\right)^2.B^2 + p_{13}.(\frac{a}{L}).B^3 \quad (3)$$

$$p_{ij}(T) = p_1.T^2 + p_2.T + p_3 \quad (4)$$

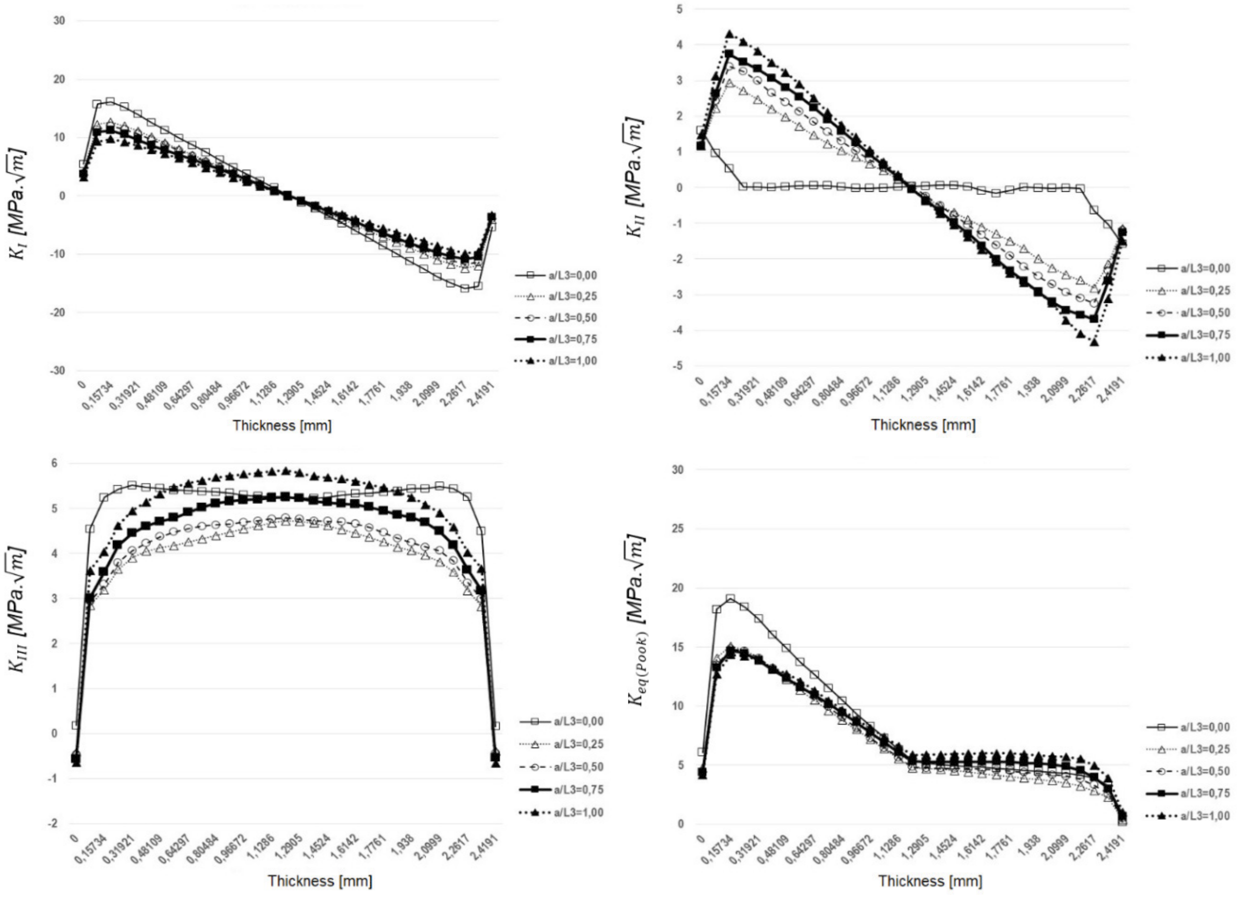

Fig. 6. Stress intensity factors, K_I, K_{II}, K_{III} and K_{eq}, at the lower crack tip (-70º) of a CT specimen with a thickness, B, equal to 2.5 mm and under an applied torque of 6 N.m.

Therefore, by using a two-step procedure (Eqs. 4 and 3), it was possible to determine the stress intensity factor values of the CT specimens under study, having into account the thickness range (2.5-10 mm), and the torsional loads considered (6 $N.m$; 7.5 $N.m$; 9 $N.m$).

Table 2. Polynomial coefficients, pij (Eq. 3), to obtain K_{eq} at upper crack tip for the three applied torques (6 N.m, 7.5 N.m, 9 N.m); B in [mm], and polynomial coefficients p_i (Eq. 4), to obtain p_{ij} (Eq. 3) at the upper crack tip. T in [N.m].

	p_{00}	p_{10}	p_{01}	p_{20}	p_{11}	p_{02}	p_{30}	p_{21}	p_{12}	p_{03}	p_{40}	p_{31}	p_{22}	p_{13}
6 N.m	52.95	-15.26	-19.42	62.1	-0.44	2.48	-46.71	-6.96	0.48	-0.106	15.81	1.54	0.277	-0.032
7.5 N.m	66.19	-19.08	-24.27	77.62	-0.555	3.106	-58.39	-8.701	0.597	-0.132	19.76	1.925	0.347	-0.040
9 N.m	79.43	-22.9	-29.13	93.14	-0.666	3.728	-70.06	-10.44	0.7164	-0.159	23.72	2.309	0.4162	-0.048

	p_{00}	p_{10}	p_{01}	p_{20}	p_{11}	p_{02}	p_{30}	p_{21}	p_{12}	p_{03}	p_{40}	p_{31}
p_1	6.05e-15	-2.2e-15	-2.22e-3	3e-15	-5e-17	2.2e-4	2.2e-3	2.2e-4	2.2e-5	-2.2e-5	2.2e-3	-2.2e-4
p_2	8.827	-2.547	-3.203	10.35	-0.074	0.411	-7.817	-1.163	0.0793	-0.0173	2.603	0.2597
p_3	-0.01	0.02	-0.12	0.02	0.0013	0.011	0.11	0.009	0.0009	-0.0012	0.11	-0.01

	p_{22}	p_{13}
p_1	2.91e-17	-4.44e-6
p_2	0.04627	-0.00532
p_3	-2e-4	-2.1e-4

4. Conclusion

The following conclusions result from the research herein presented:

- Fatigue pre-crack under torsional loading is initially subjected to mainly Mode II loading. In fact, K_{II} is the maximum SIF applied to the CT specimen (8.5 MPa.m$^{0.5}$), followed by K_{III}, which showed a maximum value of approximately 3.6 MPa.m$^{0.5}$, and K_I (1.25 MPa.m$^{0.5}$); hence, crack initiation should be Mode-II dominated and crack should grow a short distance on planes of maximum shear stress;
- After a short period of time, crack branched at an angle of ±70º and grew in Mode I under torsional loading, and K_I becomes the highest values applied at crack tip (17 MPa.m$^{0.5}$); hence, cracks will tend to grow on maximum tensile planes with higher FCGR at the external surfaces of the CT specimen and minimum FCGR at midplane;
- For the different thicknesses and torques applied during this investigation, it was noticed higher stress intensity factor values with increasing torque applied and a decrease of the stress intensity factors with the increase of the thickness of the specimens.

Acknowledgments

Authors acknowledge Fundação para a Ciência e a Tecnologia (FCT-MCTES) for its financial support via the project UIDB/00667/2020 (UNIDEMI).

References

ASTM E647 - 15e1, Standard Test Method for Measurement of Fatigue Crack Growth Rates, Annual Book of ASTM Standards, Vol. 03.01, ASTM International, U. S. A.

Barata, R., Martins, R.F., Albarran, T., Santos, T., Mourão, A. (2017). Failure analysis of a pull rod actuator of an ATOX raw mill used in the cement production process, Engineering Failure Analysis 76, 99-114.

Beretta, G., Chaves, V., Navarro, A. (2016). Biaxial fatigue tests of notched specimens for AISI 304L stainless steel, Frattura ed Integrità Strutturale, 37, 228-233.

Branco, C.M., Infante, V., Sousa e Brito, A., Martins, R.F. (2002). A failure analysis study of wet liners in maritime diesel engines, Engineering Failure Analysis, 9, 403-421.

Bugio, T., Martins, R.F., Neves, L. Leal das. (2013). Failure Analysis of Fuel Tanks of a Lightweight Ship, Engineering Failure Analysis 35, 272-285.

Collacott, R.A, (1977). *"Mechanical Fault Diagnosis"*, Chapman and Hall, Ltd., London.

Gasiak, G., Robak, G. (2010). Simulation of fatigue life of constructional steels within the mixed modes I and III loading, Fatigue Fract Engng Mater Struct 34, 389–402.

Gates, N., Fatemi, A. (2016). Friction and roughness induced closure effects on shear-mode crack growth and branching mechanisms, International Journal of Fatigue 92, 442–458.

Gomes, J., Gaivota, N., Martins, R.F., Pires da Silva, P. (2018). Failure analysis of crankshafts used in maritime V12 diesel engines, Engineering Failure Analysis 92, 466–479.

Infante, V., Branco, C.M., Martins, R. (2003), A Fracture Mechanics Analysis on the Fatigue Behaviour of cruciform joints of Duplex Stainless Steel, Fatigue Fract Engng Mater Struct, 26, pp. 791-810.

Martins, R., Branco, C.M. (2004). A fatigue and creep study in austenitic stainless steel 316L used in exhaust pipes of naval gas turbines, Fatigue Fract Engng Mater Struct 27, 861-871.

Martins, R.F., Ferreira, L., Reis, L., Chambel, P. (2016). Fatigue crack growth under cyclic torsional loading, Theoretical and Applied Fracture Mechanics 85, 56–66.

Murakami, Y., Takahashi, K., Toyama, K. (2005). Mechanism of crack path morphology and branching from small fatigue cracks under mixed loading, Fatigue Fract Engng Mater Struct 28, 49–60.

Murakami, Y. et al. (2008). Fatigue crack path and threshold in Mode II and Mode III loadings, Eng Fracture Mechanics 75, 306–318.

Ohkawa, C., Ohkawa, I. (2011). Notch effect on torsional fatigue of austenitic stainless steel: Comparison with low carbon steel, Engineering Fracture Mechanics 78, 1577–1589.

Okazaki, S., Wada, K., Matsunaga, H., Endo, M. (2017). The influence of static crack-opening stress on the threshold level for shear-mode fatigue crack growth in bearing steels, Engineering Fracture Mechanics 174, 127–138.

Pokluda, J., Slamecka, K., Šandera, P. (2010). Mechanism of factory-roof formation, Engineering Fracture Mechanics 77, 1763–1771.

Richard, H.A., Fulland, M., Sander, M. (2004). Theoretical crack path prediction, Fatigue Fract Engng Mater Struct 28, 3-12.

Schönbauer, B.M., Yanase, K., Endo, M. (2017). Influences of small defects on torsional fatigue limit of 17-4PH stainless steel, International Journal of Fatigue 100, 540–548.

Shimamura, Y. et al. (2014). Fatigue properties of carburized alloy steel in very high cycle regime under torsional loading, International Journal of Fatigue 60, 57-62.

Soares, A.G., Martins, R.F., Rodrigues Mateus, A., Pires da Silva, P. (2019). Design enhancements to a gas turbine's exhaust system used for naval propulsion, Engineering Failure Analysis 102, 20-34.

Susmel, L., Taylor, D. (2006). A simplified approach to apply the theory of critical distances to notched components under torsional fatigue loading, International Journal of Fatigue 28, 417–430.

Tanaka, K., Akiniwa, Y., Nakamura, H. (1996). J-integral approach to mode III fatigue crack propagation in steel under torsional loading, Fatigue Fract. Engng Mater. Struct. 19, 571-579.

Weiss, J., Pineau, A. (1993). Fatigue and Creep-Fatigue Damage of Austenitic Stainless Steels under Multiaxial Loading, Metallurgical Transactions A 24A, 2247-2261.